# Dual optical role of low-index injection layers for efficient polarizer-free high contrast-ratio organic light-emitting diodes

**Hyunsu Cho,[1,2] Jin Chung,[1] Jaeho Lee,[1] Eunhye Kim,[1] and Seunghyup Yoo[1,*]**

[1]*Department of Electrical Engineering, Korea Advanced Institute of Science and Technology (KAIST), 373-1 Guseong-dong, Daejeon, 305-701, South Korea*

[2]*Present address: Electronics and Telecommunications Research Institute (ETRI), 218 Gajeong-ro, Yuseong-gu, Daejeon, 305-700, South Korea*

[*]*syoo@ee.kaist.ac.kr*

**Abstract:** Polarizer-free high contrast-ratio organic light-emitting diodes (OLEDs) are explored with a structure involving a semi-reflective Cr-based bottom electrode and a dielectric-capped thin Ag top electrode. Their efficiency is shown to be improved significantly with little sacrifice in luminous reflectance by adopting low-refractive-index injection layers that can increase the effective reflectance from the bottom electrode and simultaneously reduce the loss owing to surface plasmon polariton modes. OLEDs employing a low-refractive-index injection layer exhibit improved current efficiency by up to ca. 27.4% than those using index-matched injection layers, with luminous reflectance maintained at as low as 4%.



**OCIS codes**: (230.3670) Light-emitting diodes; (230.4170) Multilayers; (310.6845) Thin film devices and applications; (310.6860) Thin films, optical properties.

## References and links

1. S. Kim, H.-J. Kwon, S. Lee, H. Shim, Y. Chun, W. Choi, J. Kwack, D. Han, M. Song, S. Kim, S. Mohammadi, I. Kee, and S. Y. Lee, "Low-power flexible organic light-emitting diode display device," Adv. Mater. **23**(31), 3511–3516 (2011).
2. B. D. Lee, Y.-H. Cho, M. H. Oh, S. Y. Lee, S. Y. Lee, J. H. Lee, and D. S. Zang, "Characteristics of contrast of active-matrix organic light-emitting diodes containing a black matrix and antireflection layers," Mater. Chem. Phys. **112**(3), 734–737 (2008).
3. V. Vaenkatesan, R. T. Wegh, J.-P. Teunissen, J. Lub, C. W. M. Bastiaansen, and D. J. Broer, "Improving the Brightness and Daylight Contrast of Organic Light-Emitting Diodes," Adv. Funct. Mater. **15**(1), 138–142 (2005).
4. D. Poitras, C.-C. Kuo, and C. Py, "Design of high-contrast OLEDs with microcavity effect," Opt. Express **16**(11), 8003–8015 (2008).
5. R. Singh, K. N. N. Unni, and A. Solanki, "Improving the contrast ratio of OLED displays: An analysis of various techniques," Opt. Mater. **34**(4), 716–723 (2012).
6. T. Ishibashi, J. Yamada, T. Hirano, Y. Iwase, Y. Sato, R. Nakagawa, M. Sekiya, T. Sasaoka, and T. Urabe, "Active matrix organic light emitting diode display based on "Super Top Emission" technology," Jpn. J. Appl. Phys. **45**(5B), 4392–4395 (2006).
7. L.-S. Hung and J. Madathil, "Reduction of ambient light reflection in organic light-emitting diodes," Adv. Mater. **13**(23), 1787–1790 (2001).
8. A. N. Krasnov, "High-contrast organic light-emitting diodes on flexible substrates," Appl. Phys. Lett. **80**(20), 3853–3855 (2002).
9. X. D. Feng, R. Khangura, and Z. H. Lu, "Metal–organic–metal cathode for high-contrast organic light-emitting diodes," Appl. Phys. Lett. **85**(3), 497–499 (2004).
10. C.-J. Yang, C.-L. Lin, C.-C. Wu, Y.-H. Yeh, C.-C. Cheng, Y.-H. Kuo, and T.-H. Chen, "High-contrast top-emitting organic light-emitting devices for active-matrix displays," Appl. Phys. Lett. **87**(14), 143507 (2005).
11. H. Cho and S. Yoo, "Polarizer-free, high-contrast inverted top-emitting organic light emitting diodes: effect of the electrode structure," Opt. Express **20**(2), 1816–1824 (2012).
12. S.-Y. Kim, J.-H. Lee, J.-H. Lee, and J.-J. Kim, "High contrast flexible organic light emitting diodes under ambient light without sacrificing luminous efficiency," Org. Electron. **13**(5), 826–832 (2012).
13. J. W. Huh, J. Moon, J. W. Lee, J. Lee, D.-H. Cho, J.-W. Shin, J.-H. Han, J. Hwang, C. W. Joo, J.-I. Lee, and H. Y. Chu, "Organic/metal hybrid cathode for transparent organic light-emitting diodes," Org. Electron. **14**(8), 2039–2045 (2013).

#234598 - $15.00 USD Received 12 Feb 2015; revised 27 Mar 2015; accepted 30 Mar 2015; published 13 Apr 2015

14. T. Schwab, S. Schubert, S. Hofmann, M. Fröbel, C. Fuchs, M. Thomschke, L. Müller-Meskamp, K. Leo, and M. C. Gather, "Eliminating micro-cavity effects in white top-emitting OLEDs by ultra-thin metallic top electrodes," Adv. Opt. Mater. **1**, 707–7013 (2013).
15. S.-M. Koo, M. D. Edelstein, Q. Li, C. A. Richter, and E. M. Vogel, "Silicon nanowires as enhancement-mode Schottky barrier field-effect transistors," Nanotechnology **16**(9), 1482–1485 (2005).
16. T.-W. Lee and Y. Chung, "Control of the surface composition of a conducting-polymer complex film to tune the work function," Adv. Funct. Mater. **18**(15), 2246–2252 (2008).
17. M. Kröger, S. Hamwi, J. Meyer, T. Riedl, W. Kowalsky, and A. Kahn, "Role of the deep-lying electronic states of MoO3 in the enhancement of hole-injection in organic thin films," Appl. Phys. Lett. **95**(12), 123301 (2009).
18. Y.-K. Kim, J. W. Kim, and Y. Park, "Energy level alignment at a charge generation interface between 4,4'-bis(N-phenyl-1-naphthylamino)biphenyl and 1,4,5,8,9,11-hexaazatriphenylene-hexacarbonitrile," Appl. Phys. Lett. **94**(6), 063305 (2009).
19. R. Liu, C. Xu, R. Biswas, J. Shinar, and R. Shinar, "MoO3 as combined hole injection layer and tapered spacer in combinatorial multicolor," Appl. Phys. Lett. **99**(9), 093305 (2011).
20. H. You, Y. Dai, Z. Zhang, and D. Ma, "Improved performances of organic light-emitting diodes with metal oxide as anode buffer," J. Appl. Phys. **101**(2), 026105 (2007).
21. M. Furno, R. Meerheim, S. Hofmann, B. Lüssem, and K. Leo, "Efficiency and rate of spontaneous emission in organic electroluminescent devices," Phys. Rev. B **85**(11), 115205 (2012).
22. C. Fuchs, T. Schwab, M. Wieczorek, M. C. Gather, S. Hofmann, K. Leo, and R. Scholz, "Surface plasmon polariton modification in top-emitting organic light-emitting diodes for enhanced light outcoupling," Proc. SPIE **9183**, 91831Z (2014).

## 1. Introduction

Contrast ratio (CR) is an important parameter determining the quality of a display and is regarded as one of the most critical factors that make organic light-emitting diodes (OLEDs) stand out among the competing display technologies [1,2]. With the self-emitting properties of OLEDs, complete "black" can be realized in principle by turning off a given pixel in OLED-based displays, endowing themselves with a competitive edge against conventional displays such as liquid crystal displays that rely on modulation of a rear light source. However, CR in a real environment is determined not only by the performance of the display itself but also by the ambient light condition. The reflection of outdoor daylight or indoor lighting is especially a main factor that hinders a given display technology from exhibiting its ultimate CR value. In OLED-based displays, a circular polarizer is thus attached onto the emitting side of a substrate or a superstrate to suppress the reflection of ambient light coupled with a metallic electrode [3]. However, this specialty film can incur a relatively high cost and, moreover, causes inevitable power loss of 50-60% due to its finite transmittance and the unpolarized nature of the light from OLEDs. It may also be unsuitable when it comes to highly flexible devices due to its relatively large thickness [4, 5].

Many studies have thus been devoted to development of polarizer-free high CR OLEDs. For example, a microcavity-based structure with a matching color filter has been demonstrated as a scheme where high CR (low reflection) can be achieved with little power loss [1,6]; but this scheme also tends to increase the overall cost due to rather complicated patterning processes involved. Other methods include those based on a completely absorbing or black back electrode and those based on an approach where the whole structure of an OLED is considered as a multilayer stack and optimized for broadband anti-reflection (AR) [7–12]. In particular, the latter tries to attain complete destructive interference for ambient light reflected from various layers in OLEDs by careful intensity balancing and phase reversal. In such a scheme, relative phase between major reflected components is varied by controlling the thicknesses of participating layers, and intensity balancing is typically done by introducing semi-absorbing layer either in the top part [12] or in the bottom side [10, 11]. In this way, reduction of emitted optical power is mitigated while still suppressing the reflection of ambient light even with a relatively simple structure and process. Motivated by these benefits, we previously demonstrated a polarizer-free, high-CR OLED based on a top-emitting configuration in which a bottom electrode of Cr played a role as a semi-absorbing/ low-reflective layer and a high-index dielectric layer of ZnS tuned the transmittance of a top electrode (via its thickness variation) and thus allowed for balancing of the intensities of two major reflected components. Luminous reflectance of OLEDs ($R_{\mathrm{OLED}}^{(L)}$) was achieved as low as

#234598 - $15.00 USD Received 12 Feb 2015; revised 27 Mar 2015; accepted 30 Mar 2015; published 13 Apr 2015

3.16%, and its luminous current efficiency was demonstrated to be comparable to or slightly higher than the reference device with a circular polarizer.

In this work, we show that the efficiency of these high-CR OLEDs can further be improved significantly with little sacrifice in luminous reflectance. An emphasis is placed on the optical role of low-refractive-index injection layers that can increase the effective reflectance from the bottom electrode to a near-optimal value and, at the same time, reduce the loss owing to surface plasmon polariton (SPP) modes. Polarizer-free high CR OLEDs employing a low refractive index injection layer is shown to exhibit improved current efficiency by ca. 56.7% (ca. 27%) than those using a high refractive index metal-oxide injection (index-matched organic injection) layer with luminous reflectance maintained at as low as 4%. As an added benefit, these OLEDs are demonstrated to have Lambertian emission characteristics and show no angular spectral shift typical to top-emitting OLEDs.

## 2. Experimental

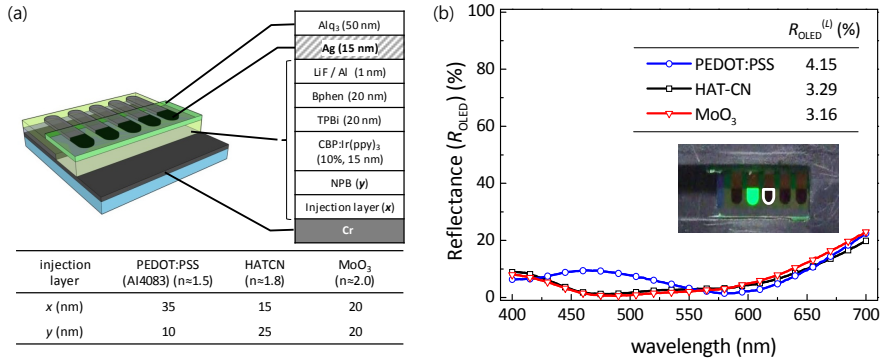


| injection layer | PEDOT:PSS (Al4083) (n≈1.5) | HATCN (n≈1.8) | $MoO_3$ (n≈2.0) |
|---|---|---|---|
| *x* (nm) | 35 | 15 | 20 |
| *y* (nm) | 10 | 25 | 20 |

Fig. 1. (a) Schematic diagrams of OLED structures under study: (b) Measured reflectance spectra of OLEDs ($R_{OLED}$) under study. Inset: photograph of the proposed OLED device. The white line in the photograph is a guide to eye indicating the active region. Luminous reflectance values of the OLED devices $R_{OLED}^{(L)}$ are also shown for each case.

Figure 1(a) depicts the proposed high-CR OLED structure based on a phosphorescent emitter of fac-tris(2-phenylpyridine) iridium ($Ir(ppy)_3$) doped in a host of 4,4- *N*,*N*′-dicarbazole-biphenyl (CBP). Cr layers were deposited as bottom electrodes on precleaned substrates by sputtering. As a hole injection layer from the bottom Cr electrode into a hole transport layer of *N*,*N*′-Di(1-naphthyl)-*N*,*N*′-diphenyl-(1,1′-biphenyl)-4,4′-diamine (NPB), conducting polymers of poly(3,4-ethylenedioxythiophene):poly(styrenesulfonate) (PEDOT:PSS, 35 nm) were spin-coated, or $MoO_3$ (20 nm) or 2,3,6,7,10,11-hexacyano-1,4,5,8,9,12-hexaazatriphenylene (HAT-CN, 15 nm) were thermally evaporated under high vacuum conditions ($2 \times 10^{-6}$ torr) on top of Cr electrodes. The refractive indices of PEDOT:PSS (ca. 1.5) and $MoO_3$ (ca. 2.0) are smaller and larger than those of organic layers (1.7-1.8), respectively, and that of HAT-CN is similar to typical organic semiconductor materials. The remaining multilayer stack had a configuration of NPB (*y* nm) / CBP:$Ir(ppy)_3$ (15 nm) / 2,2,2-(1,3,5-benzenetriyl)tris-[1-phenyl-1H-benzimidazole] (TPBi, 20 nm)/ 4,7-diphenyl-1,10-phenanthroline (Bphen, 20 nm)/ LiF (1 nm) /Al (1.5 nm)/ Ag (15 nm)/ tris-(8-hydroxyquinoline)aluminum ($Alq_3$, 50 nm). The ultrathin Al works as a wetting layer, promoting the formation of smooth Ag layers [13, 14]. $Alq_3$ capping layer is used to suppress the reflection of ambient light mainly by varying the transmittance of top electrodes in such a way the balance between major reflected lights may be achieved for complete destructive interference [11]. The total thickness of layers between two electrodes is important to fulfill the phase condition required for destructive interference, which was controlled in this work through the thickness of a hole transporting layer (HTL) (*y*) for a given thickness of a hole injection layer (HIL) (*x*).

#234598 - $15.00 USD Received 12 Feb 2015; revised 27 Mar 2015; accepted 30 Mar 2015; published 13 Apr 2015

## 3. Results and discussion

Figure 1(b) shows the reflectance spectra of OLEDs under study. With the properly chosen thicknesses of HIL ($x$) and HTL ($y$) shown at the bottom of Fig. 1(a), the total reflectance values of light incident on OLEDs are kept less than 10-20% throughout the visible spectral range, resulting in the $R_{OLED}^{(L)}$ [4] ( = the average reflectance of an OLED weighted for photopic response under illumination from the standard white light source) less than ca. 4%. In OLEDs where the luminance of "off" pixel is negligible, CR is essentially given by CR = 1 + $L_{on}/[R_{OLED}^{(L)} L_{amb}]$ where $L_{on}$ and $L_{amb}$ are the luminance of an OLED and ambience, respectively. Since $L_{on}/L_{amb}$ is operation-condition-dependent, it is $R_{OLED}^{(L)}$ that ultimately governs the CR of an emissive display. The observed level of $R_{OLED}^{(L)}$ is comparable to that of conventional OLEDs adopting a circular polarizer.

Current density ($J$)-voltage ($V$)-luminance ($L$) characteristics are shown in Fig. 2(a). Though the work function of Cr is not so high (~4.5 eV) to be used as an anode [15], it can be seen that all the HILs under comparison function properly, leading to a similar operating voltage of approximately 2.7 V and 4.5 V for luminance of 1 cd/m$^2$ and 1,000 cd/m$^2$, respectively, in all devices. PEDOT:PSS can improve the direct charge injection to HTL due to its high work function [16]. On the other hand, HAT-CN and $MoO_3$ form an efficient charge carrier generation interface because their lowest unoccupied molecular orbital (LUMO) is very close to the Fermi level and the highest occupied molecular orbital (HOMO) of NPB [17, 18]. Despite the different mechanisms for hole injection, the HILs using in this study work efficiently. $J$-$V$ characteristics of those devices overlap one another relatively well, ensuring that the difference in luminous current efficiency, if any, comes mainly from the optical properties. It is worth to mention that the thickness of HAT-CN and $MoO_3$ usually does not have to be thicker than 10 nm but it was chosen to be so for the sake of a fair comparison because the thickness of a spin-coated PEDOT:PSS layer is rather difficult to reduce below 10 nm. Though the $MoO_3$ less than 1 nm is often used, a few tens of nanometer thick $MoO_x$ was also shown to be a good injection and spacer layer for OLEDs [19, 20]. If the thickness of HAT-CN and $MoO_3$ had been chosen to be thinner than 10 nm, too thick a HTL would have been required to achieve a phase reversal condition required for a destructive interference and low $R_{OLED}^{(L)}$ [11] and in turn would have compromised the electrical property (e.g. increased voltage).

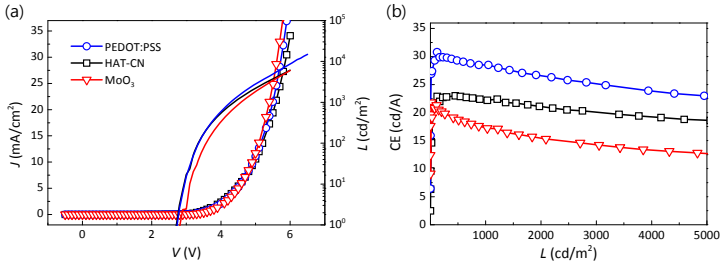


Fig. 2. Device performance of high CR OLEDs with PEDOT:PSS (circle; blue), HAT-CN (square; black), and $MoO_3$ (triangle; red) injection layers: (a) Current density ($J$)-voltage ($V$)-luminance ($L$) characteristics; (b) current efficiency (CE) - $L$ characteristics.

The current efficiency (CE) of OLEDs is shown in Fig. 2(b). It can be observed that, even with similar electrical characteristics, CE differs greatly depending on HILs. It should be noted that CE is in the opposite order of the refractive index of HILs ($n_{HIL}$): the devices with PEDOT:PSS ($n_{HIL}$ ~1.5) and with HAT-CN ($n_{HIL}$ ~1.8) exhibit CE of 29.3 cd/A and 23 cd/A at $L$ of 500 nits, which is 56.7% and 23% enhancement, respectively, from 18.7 cd/A obtained for $MoO_3$-based device ($n_{HIL}$ ~2.0) at the same $L$. It turns out that the low refractive index of PEDOT:PSS is very effective in increasing the reflectance of the bottom electrode ($R_{bot}$) as it can work like a high-reflection (HR) coating while the high refractive index of $MoO_3$ tends to decrease $R_{bot}$. [See Fig. 3(a)].

#234598 - $15.00 USD Received 12 Feb 2015; revised 27 Mar 2015; accepted 30 Mar 2015; published 13 Apr 2015

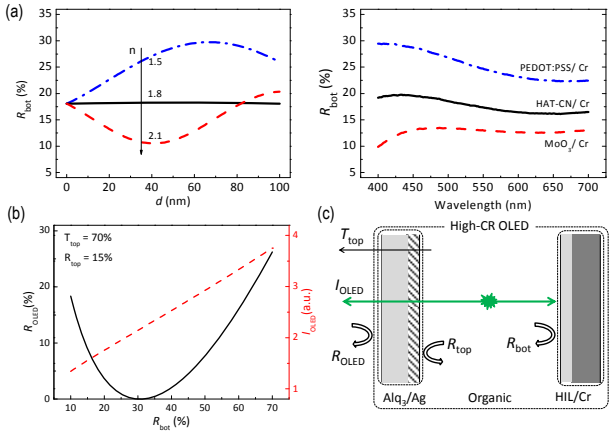


Fig. 3. Optical simulation results for proposed bottom electrodes and high CR OLED structures. (a) (left) The reflectance of bottom electrode ($R_{bot}$) vs. HIL thickness ($d$) for HILs with refractive indices ($n$) of 1.5, 1.8, and 2.0 at λ of 520 nm. (right) $R_{bot}$ spectra obtained for HILs under study. (b) Scaling behavior of the reflectance ($R_{OLED}$) and output intensity ($I_{OLED}$) of OLEDs vs. $R_{bot}$ assuming that the transmittance and the reflectance of top electrode combination ($Alq_3$ capped Ag) for light incident from organic layers are 70% and 15%, respectively. (c) Schematic diagram illustrating the definition of various reflectance and transmittance terms.

Efficiency in this type of polarizer-free high CR OLEDs is mainly influenced positively by $R_{bot}$ because the increased portion of the light internally emitted toward the bottom electrode can be utilized with a high $R_{bot}$. Of course, the improved efficiency by the increased $R_{bot}$ would not be meaningful if it tends to increase $R_{OLED}^{(L)}$ for incident light. Figure 3(b) presents the scaling behavior of the reflectance ($R_{OLED}$) and output intensity ($I_{OLED}$) of an OLED vs. $R_{bot}$ in which the thickness of the organic layer is assumed to satisfy the *phase* condition for destructive interference of light incident onto and reflected from the OLED. [See Ref. 11 and Fig. 3(c) for details.] It shows that the $R_{OLED}$ can still be maintained low even with the increased $R_{bot}$ provided that $R_{bot}$ is not excessively high for a given top electrode transmittance. This is mainly because $R_{OLED}$ varies slowly following a parabolic function of $R_{bot}$ near its minimum and because the intensity balance between major reflected components leading to the minimum $R_{OLED}$ is obtained with a relatively high $R_{bot}$ [ = ~30% in the example shown in Fig. 3(b)]. It is also noteworthy that the cavity resonant effect is still weak, despite the enhanced $R_{bot}$, such that the angular emission exhibits near-Lambertian characteristics with little spectral shift [See Figs. 4(a) and 4(b)].

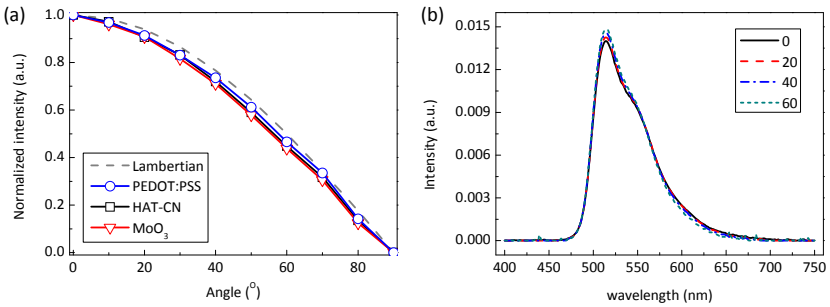


Fig. 4. (a) Angular intensity characteristics of high CR OLEDs with HAT-CN, PEDOT:PSS, and $MoO_3$. (b) Measured intensity spectra of OLEDs with PEDOT:PSS as HIL under study for several viewing angles.

The measured enhancement in CE, however, turns out to be quite larger than the value expected from a simplified calculation based on a cavity resonance effect (Model 1), [red dashed line in Fig. 3(b)] [11] in which CE enhancement is mainly governed by $R_{bot}$.

#234598 - $15.00 USD Received 12 Feb 2015; revised 27 Mar 2015; accepted 30 Mar 2015; published 13 Apr 2015

Under Model 1, the increase in $R_{bot}$ ($\lambda$ = 520 nm) from 13.3% ($MoO_3$) to 18.1% (HAT-CN) and 26.0% (PEDOT:PSS) is expected to result in only 14.3% and 35.4% enhancement in CE, respectively. [See Table 1 for summary] This discrepancy with the experimentally observed enhancement calls for more rigorous analysis for a complete account. With this in mind, full analysis has been carried out based on a dipole emitter model (Model 2) that takes into account the resonance effect considering the effect of surrounding media on radiative decay rate (Purcell effect) as well as excitations to various modes (e.g. wave-guided (WG) modes; SPP modes) [21].

**Table 1. Efficiency comparison of the proposed high CR OLEDs**

| | **Experiment** | | **Model 1**[a] | | **Model 2**[b] | |
|---|---|---|---|---|---|---|
| | CE (cd/A) | Enhancement[c] (%) | Intensity (a.u.) | Enhancement[c] (%) | $\eta_{out}$ (%) | Enhancement[c] (%) |
| $MoO_3$ | 18.7 | 0.0 (–18.7) | 1.47 | 0.0 (–12.5) | 5.68 | 0.0 (–19.8%) |
| HAT-CN | 23.0 | 23.0 (0.0) | 1.68 | 14.3 (0.0) | 7.08 | 24.6 (0.0) |
| PEDOT:PSS | 29.3 | 56.7 (27.4) | 1.99 | 35.4 (18.5) | 8.64 | 52.1 (22.0%) |

[a] calculation based on a simplified model for a cavity resonance effect [11].

[b] calculation based on a full dipole emitter model that includes resonance effect considering Purcell effect as well as various mode excitations [21].

[c] enhancement over $MoO_3$-based device. Enhancement over HATCN-based devices is also shown inside parenthesis.

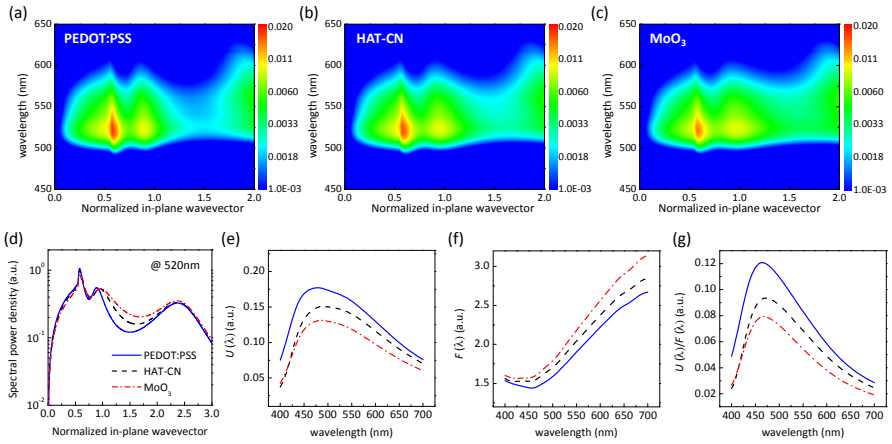


Fig. 5. Power dissipation spectra weighted with the emitter spectrum (arbitrary units) per unit normalized in-plane wavevector ($u$) and unit wavelength of OLEDs with (a) PEDOT:PSS, (b) HAT-CN, and (c) $MoO_3$. (d) Power dissipation spectra at the wavelength of 520 nm. Wavelength dependence of the power spectra calculated for the same OLED device; (e) outcoupled power $U(\lambda)$, (f) total radiated power $F(\lambda)$, also called "Purcell factor," and (g) $U(\lambda)/F(\lambda)$, which is proportional to the outcoupling efficiency at $\lambda$.

Figures 5(a)-5(c) show the calculated power dissipation simulation spectra as a function of normalized in-plane wave number for devices under study. It is noted that the plots are quite different in the region where normalized in-plane wave vector is larger than 1, which corresponds to evanescent or SPP modes; the power coupled to the opaque Cr metal SPP modes is smaller for OLEDs with lower-index HILs than those with higher-index HILs due to the shift of the SPP to smaller wavenumber [See Fig. 5(d)]. (The SPP coupled to the transparent top Ag electrode at normalized in-plane wavenumber of ca. 2.4 is almost the same.) SPP modes are avoided usually by increasing the distance between an emitting layer and a metal electrode at the expense of increased WG modes. However, a low refractive index layer placed adjacent to the metal electrode can also effectively reduce the power loss coupled to SPP modes [22]; the total optical thickness in this case does not vary significantly, and thus the WG modes remain similar. The two relevant

#234598 - $15.00 USD Received 12 Feb 2015; revised 27 Mar 2015; accepted 30 Mar 2015; published 13 Apr 2015

quantities in Model 2 - the total radiated power $F(\lambda)$, also known as Purcell factor, and the outcoupled power $U(\lambda)$ - provide a means for quantitative evaluation of outcoupling efficiency ($\eta_{out}(\lambda)$), which is proportional to $U(\lambda)$ / $F(\lambda)$ [See Fig. 5(e)-5(g)] [21]. Under Lambertian approximation, the relative ratio of $U(\lambda)$ among devices under study corresponds to that of intensity enhancement ratio calculated in Fig. 3(b) by Model 1. Together with the enhancement in $U(\lambda)$ due to the increased $R_{bot}$, $F(\lambda)$ decreased by the reduced SPP leads to the highest $\eta_{out}$ (and thus highest external quantum efficiency) for PEDOT:PSS based OLEDs, as shown in Fig. 5(g). As can be seen in Table 1, the ratios of $\eta_{out}$ enhancement calculated in this way exhibit a good agreement with the experimentally obtained efficiency enhancement, confirming the validity of the present analysis.

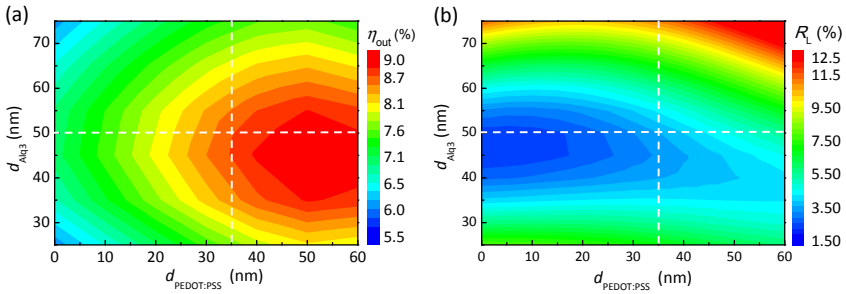


Fig. 6. (a) Outcoupling efficiency calculated by Model 2 and (b) $R_{OLED}^{(L)}$ vs. capping ($Alq_3$) layer thickness ($d_{Alq3}$) and PEDOT:PSS thickness ($d_{PEDOT:PSS}$). The cross point corresponds to the present device structure. The thickness of the organic HTL was chosen such that the overall optical thickness including HIL remained constant.

Figure 6(a) and 6(b) present contour plots for outcoupling efficiency calculated by Model 2 and $R_{OLED}^{(L)}$ vs. capping ($Alq_3$) layer thickness ($d_{Alq3}$) and PEDOT:PSS thickness ($d_{PEDOT:PSS}$). It can be seen that a better efficiency may be achieved when $d_{PEDOT:PSS}$ increases to 50-60 nm. Nevertheless, there is also a limitation because increased $R_{bot}$ with increased $d_{PEDOT:PSS}$ can break the intensity balance between two major reflecting components, thus compromising a complete destructive interference and increasing $R_{OLED}^{(L)}$ even though the thickness of organic layers is chosen such that the overall optical thickness of organic plus injection layers are kept same. Such a trend is confirmed in Fig. 6(b), illustrating the importance of an optical design balancing both low $R_{OLED}^{(L)}$ and high efficiency.

## 4. Conclusions

Polarizer-free high CR OLEDs were studied based on a structure involving a semi-reflective Cr-based bottom electrode and a dielectric-capped thin Ag top electrode. Noting that the forward luminous efficiency is mainly governed by reflectance from the bottom electrode ($R_{bot}$) in this type of OLEDs, PEDOT:PSS was used as a low refractive index HIL on top of the Cr electrode. This effectively increased $R_{bot}$ as it functioned like a high-reflection (HR) coating. Despite the increased $R_{bot}$, the total luminous reflectance of the whole OLED structure ($R_{OLED}^{(L)}$) still remained low because $R_{OLED}^{(L)}$ depended on $R_{bot}$ parabolically near its minimum. The rigorous analysis based on a dipole emitter and its power dissipation revealed that the low-index HIL enhance the efficiency of the proposed OLEDs not only by the increased $R_{bot}$ but also by the reduction of SPP modes. We believe the method proposed in this work can open up the possibility to improve the efficiency of polarizer-free OLEDs without compromise in $R_{OLED}^{(L)}$, achieving a good balance among high contrast and efficiency.


## Acknowledgment

This work was supported by the RFID R&D program of MKE/KEIT under grant No. 10035225 (“Development of core technology for high performance AMOLED on plastic”).


#234598 - $15.00 USD Received 12 Feb 2015; revised 27 Mar 2015; accepted 30 Mar 2015; published 13 Apr 2015